Finite Volume Central Schemes for Three-Dimensional Ideal MHD

P. Arminjon and R. Touma

Summary. We present second-order accurate central finite volume methods adapted here to three-dimensional problems in ideal magnetohydrodynamics. These methods alternate between two staggered grids, thus leading to Riemann solver-free algorithms with relatively favorable computing times.

The original grid considered in this paper is Cartesian, while the dual grid features either Cartesian or diamond-shaped oblique dual cells.

The $\mathrm{div}\cdot\mathbf{B} = 0$ constraint on the magnetic field is enforced with a suitable adaptation of the constrained transport method to our central schemes.

Numerical experiments show the feasibility of these methods and our results are in good agreement with existing results in the literature.

1 Introduction

The equations of ideal MHD, which consist of the conservation laws for the mass density ρ, momentum $\rho\mathbf{v}$, total energy ρe as well as Faraday's induction law, can be written as [JT64]

$$\frac{\partial}{\partial t}\begin{bmatrix}\rho\\ \rho\mathbf{v}\\ \rho e\\ \mathbf{B}\end{bmatrix} + \nabla\cdot\begin{bmatrix}\rho\mathbf{v}\\ \rho\mathbf{v}\mathbf{v} + I(p+\frac{\mathbf{B}\cdot\mathbf{B}}{2}) - \mathbf{B}\mathbf{B}\\ (\rho e + p + \frac{\mathbf{B}\cdot\mathbf{B}}{2})\mathbf{v} - (\mathbf{v}\cdot\mathbf{B})\mathbf{B}\\ \mathbf{v}\mathbf{B} - \mathbf{B}\mathbf{v}\end{bmatrix} = 0, \tag{1}$$

where $\mathbf{B}$ is the magnetic field and I is the (3×3) identity matrix; the thermal pressure is computed from an ideal gas equation of state,

$$P = (\gamma-1)(\rho e - \frac{1}{2}\rho|\mathbf{v}|^2 - \frac{1}{2}|\mathbf{v}|^2), \tag{2}$$

where γ denotes the ratio of specific heats.

2 3D Central Schemes with Cartesian or Diamond-Shaped Dual Cells

The 3D-numerical schemes considered here are based on our two-dimensional finite volume schemes [AV95][ASV95], inspired from the Nessyahu–Tadmor one-dimensional central scheme [NT90].

We consider the three-dimensional hyperbolic system:

$$\overrightarrow{U}_t + \nabla \cdot \mathbf{F} = \overrightarrow{U}_t + \overrightarrow{f}_x + \overrightarrow{g}_y + \overrightarrow{h}_z = 0, \quad t > 0, \tag{3}$$

with initial condition $\overrightarrow{U}(x, y, z, t = 0) = \overrightarrow{U}_0(x, y, z)$.

The computational domain is a uniform parallelepiped-shaped grid. We consider here the case of Cartesian dual cells. Starting from cell-average values $\overrightarrow{U}^n_{ijk}$ defined, at time t^n on the Cartesian cells $C_{i,j,k} \equiv [x_{i-1/2}, x_{i+1/2}] \times [y_{j-1/2}, y_{j+1/2}] \times [z_{k-1/2}, z_{k+1/2}]$ of the original grid, we compute new values $\overrightarrow{U}^{n+1}_{i+1/2,j+1/2,k+1/2}$ defined, at time t^{n+1}, on the staggered Cartesian dual cells $D_{i+1/2,j+1/2,k+1/2} = [x_i, x_{i+1}] \times [y_j, y_{j+1}] \times [z_k, z_{k+1}] \equiv \mathcal{D}_{i,j,k}$ for simplicity (Fig. 1, dashed line cube) by integrating (3) on $\mathcal{D}_{i,j,k} \times [t^n, t^{n+1}]$ and applying Green's theorem, obtaining

$$Vol(\mathcal{D}_{i,j,k})\overrightarrow{U}^{n+1}_{i+1/2,j+1/2,k+1/2}) \equiv \int_{\mathcal{D}_{i,j,k}} \overrightarrow{U}(x, y, z, t^{n+1})dV =$$

$$\int_{\mathcal{D}_{i,j,k}} \overrightarrow{U}(x, y, z, t^n)dV - \int_{t_n}^{t_n+1} \int_{\partial\mathcal{D}_{i,j,k}} (\overrightarrow{f}\, n_x + \overrightarrow{g}\, n_y + \overrightarrow{h}\, n_z)dAdt \tag{4}$$

where $\overrightarrow{n} = (n_x, n_y, n_z) =$ unit outer normal to $\partial\mathcal{D}_{i,j,k}$ (boundary of $\mathcal{D}_{i,j,k}$).

Applying piecewise linear interpolants in x, y, z with slopes controlled by van Leer's MC-θ limiter, and a midpoint quadrature for the time integration leads to second-order accuracy; the intermediate time value $\overrightarrow{U}^{n+1/2}$ is

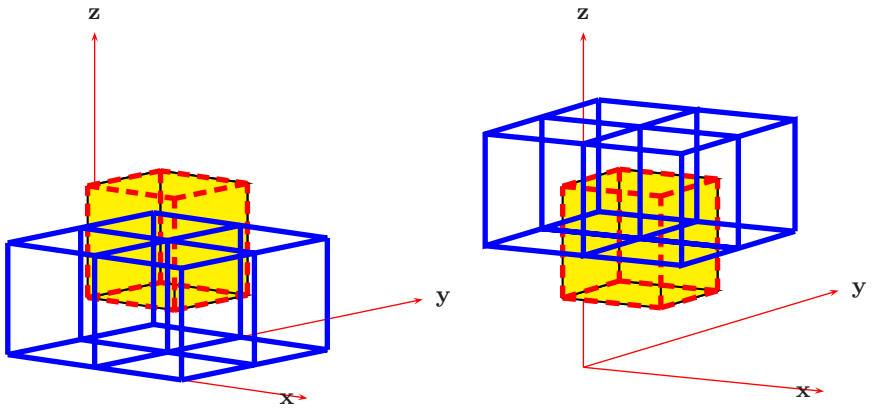

Fig. 1. One dual cell (*dashed line cube*) intersects two layers of four original cells (*solid line cubes*)

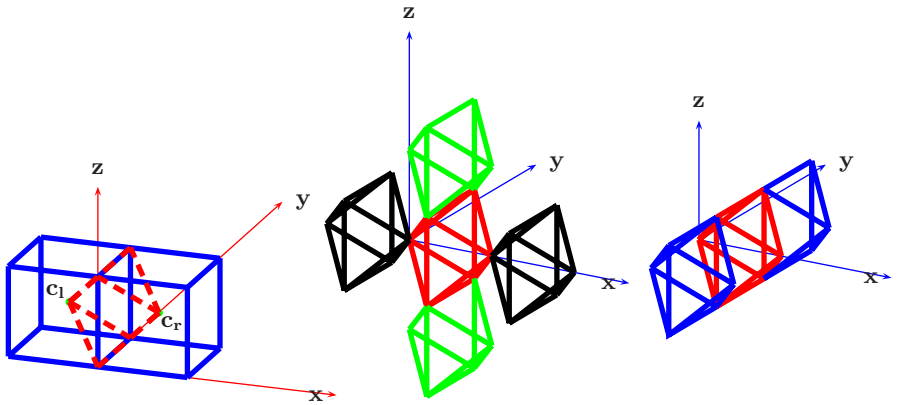

Fig. 2. (*Left*) Two Cartesian cells $C_{i,j,k}$, $C_{i+1,j,k}$ and dual diamond cell $D_{i+1/2,j,k}$. (*Middle and right*) Six diamond dual cells along the x and z directions (*middle*) and the y direction (*right*) are required to compute $\nabla \cdot B^{n+1}_{i+1/2,j,k}$

obtained using an explicit Euler time discretization of (3) ([T05]). A similar second time step then uses the values $\overrightarrow{U}^{n+1}_{i+1/2,j+1/2,k+1/2}$ to construct values U^{n+2}_{ijk} on the original cells C_{ijk}. The scheme using diamond-shaped dual cells $\mathcal{D}_{i+1/2,j,k}$ (or $\mathcal{D}_{i,j+1/2,k}$ and $\mathcal{D}_{i,j,k+1/2}$, respectively) (see Fig. 2, left) proceeds in a similar way, see [AT05, TA06].

3 A Constrained Transport Divergence Treatment for 3D Central Schemes (CTCS)

Based on experimental observations, the expression of the magnetic field $\mathbf{B}$ given by Biot and Savart's law [PP55] leads to the existence of a magnetic vector potential $\mathbf{A}$ such that curl$\mathbf{A} = \mathbf{B}$ and therefore to Maxwell's equation $\nabla \cdot \mathbf{B} = 0$, which must be satisfied. Faraday's law guarantees that if the initial magnetic field is solenoidal, it remains divergence-free at upcoming time. But the accumulation of numerical errors most often leads to a numerical solution that does not satisfy the $\nabla \cdot \mathbf{B} = 0$ constraint. Among many useful methods to restore a solenoidal $\mathbf{B}$, Evans and Hawley's Constrained Transport (CT) approach [EH88] has proven to be very efficient. Since our schemes use two staggered grids, none of the existing versions of the CT method can be applied directly. Our own approach to satisfy the divergence constraint, inspired from the CT method, is based on a specific discretization of the induction equation on both the original and staggered dual grids. In this paper we describe our Constrained Transport method for Central Schemes (CTCS) in the case of diamond-shaped dual cells $\mathcal{D}_{i+1/2,j,k}$.

Let $\overrightarrow{U}^n_{ijk}$ denote the solution at time t^n on the Cartesian cell C_{ijk}, and $\overrightarrow{U}^{n+1}_{i+1/2,j,k}$ the solution at time t^{n+1} on the staggered dual cell $\mathcal{D}_{i+1/2,j,k}$. We suppose that the constraint $\nabla\cdot\mathbf{B}^n_{ijk}=0$ is satisfied, i.e., the central difference discretization of the divergence operator satisfies

$$\nabla\cdot\mathbf{B}^n_{i,j,k}\approx\frac{B^{n,x}_{i+1,j,k}-B^{n,x}_{i-1,j,k}}{2\Delta x}+\frac{B^{n,y}_{i,j+1,k}-B^{n,y}_{i,j-1,k}}{2\Delta y}+\frac{B^{n,z}_{i,j,k+1}-B^{n,z}_{i,j,k-1}}{2\Delta z}=0. \tag{5}$$

Performing the step $t^n\to t^{n+1}$, we obtain a solution $\overrightarrow{U}^{n+1}_{i+1/2,j,k}$ for the dual cells $\mathcal{D}_{i+1/2,j,k}$ whose magnetic field part, denoted by $\mathbf{B}^*$, must be treated to obtain a divergence-free magnetic field $\mathbf{B}^{n+1}$. We first compute the electric field $\mathbf{E}^{n+1/2}_{i+1/2,j,k}=(\Omega^x,\Omega^y\Omega^z)^{n+1/2}_{i+1/2,j,k}$ at time $t^{n+1/2}$ using the data at time t^n and t^{n+1}, on the original and the dual staggered grids, respectively, as follows:

$$\begin{aligned}\mathbf{E}^{n+1/2}_{i+1/2,j,k}&=-(\mathbf{v}\times\mathbf{B})^{n+1/2}_{i+1/2,j,k}\\&\cong-\frac{1}{2}\left[(\mathbf{v}^{n+1}\times\mathbf{B}^*)_{i+1/2,j,k}+\frac{1}{2}\big\{(\mathbf{v}\times\mathbf{B})^n_{i,j,k}+(\mathbf{v}\times\mathbf{B})^n_{i+1,j,k}\big\}\right].\end{aligned} \tag{6}$$

This discretization will ensure second-order accuracy with respect to time. We then discretize the induction equation $\partial_t\mathbf{B}+\nabla\times\mathbf{E}=0$ on the $\mathcal{D}_{i+1/2,j,k}$-type dual cells using the following centered differences:

$$\mathbf{B}^{n+1,x}_{i+1/2,j,k}=\frac{1}{2}(B^{n,x}_{i,j,k}+B^{n,x}_{i+1,j,k})-\Delta t\frac{\Omega^{n+1/2,z}_{i+1/2,j+1,k}-\Omega^{n+1/2,z}_{i+1/2,j-1,k}}{2\Delta y}+\Delta t\frac{\Omega^{n+1/2,y}_{i+1/2,j,k+1}-\Omega^{n+1/2,y}_{i+1/2,j,k-1}}{2\Delta z}, \tag{7}$$

with similar expressions for the y and z components [TA06]. This special discretization of the induction equation and the above interpolation for the electric field at the intermediate time $t^{n+1/2}$ preserve the second-order accuracy of the base scheme.

It can be shown that these choices lead to

$$\nabla\cdot\mathbf{B}^{n+1}_{i+1/2,j,k}=\frac{1}{2}\big\{\nabla\cdot\mathbf{B}^n_{i,j,k}+\nabla\cdot\mathbf{B}^n_{i+1,j,k}\big\}=0, \tag{8}$$

since the magnetic field $\mathbf{B}$ was assumed to be solenoidal at time t^n. A similar treatment of the magnetic field on the cells of type $\mathcal{D}_{i,j+1/2,k}$ and $\mathcal{D}_{i,j,k+1/2}$ then guarantees a divergence-free magnetic field $\mathbf{B}^{n+1}$ at time t^{n+1}.

The CTCS divergence treatment in the case of Cartesian dual cells proceeds in a similar way [TA06].

4 Numerical Experiments

Because of the use of two staggered dual grids, which results in a restriction on the time step, our numerical experiments have been performed with a CFL number of 0.475.

1. Our first test is an Orszag–Tang-type problem [DW98, T00, Z04], which is itself a modification of a problem proposed by Nodes et al. [NGL04]. The initial data are as follows: $\rho(x,y,z) = \rho_0,\ p(x,y,z) = p_0,\ \mathbf{u}(x,y,z) = -\sin y \sin z\ \mathbf{i} + \sin x \sin z\ \mathbf{j},\ \mathbf{B}(x,y,z) = -\sin y \sin z\ \mathbf{i} + \sin(2x) \sin z\ \mathbf{j} + \sin(2x) \sin y\ \mathbf{k}$, with $0 \le x,y,z \le 2\pi,\ \rho_0 = 25/36$ and $p_0 = 5/3$. $\mathbf{i}$, $\mathbf{j}$, and $\mathbf{k}$ are the unit vectors in the x, y, and z directions, respectively. We have computed the solution at time $t = 0.5$ on 100^3 gridpoints using the Cartesian dual cell scheme; thanks to our CTCS divergence treatment, the maximum absolute value of the divergence observed for this Orszag–Tang vortex problem is of the order of 10^{-14}. Figure 3 (left) shows the contours of the mass density in the plane $x = \pi/2$ at time $t = 0.5$. If we do not apply the CTCS divergence treatment the base scheme can still reach the final time without showing instabilities: we have also solved this problem using the diamond dual cell scheme on 50^3 gridpoints, without CTCS divergence treatment. Figure 3 (right) shows the plots along the line $y = z = \pi/2$ of the energy obtained with the Cartesian dual cell with CTCS treatment and on both 100^3 grid (solid line) and 50^3 grid (dashed line), and with the diamond dual scheme without CTCS divergence treatment (dotted line). We find that the numerical results obtained without CTCS treatment are still reasonable, and the maximum of the absolute value of $\nabla \cdot \mathbf{B}$ observed in this case is 3.124×10^{-1}. Comparing the dotted line with the dashed line, the necessity of a divergence treatment is more apparent in the neighborhood of local extremas.

2. Our second test is a three-dimensional adaptation of a classical 2D MHD shock-cloud interaction problem [10,24,27,20]. The computational domain $(x,y,z) \in [0,1]^3$ is uniformly discretized using 100^3 gridpoints. Two constant states $U_l = [3.86859,\ 11.2536,\ 0,\ 0,\ 167.345,\ 0,\ 2.1826182,\ -2.1826182]$ and $U_r = [1,\ 0,\ 0,\ 0,\ 1,\ 0,\ 0.56418958,\ 0.56418958]$ are separated by the plane

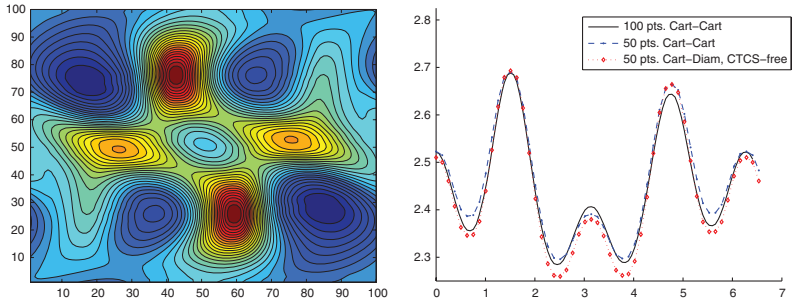

Fig. 3. (*Left*) Mass density contours in the plane $z = \pi/2$. (*Right*) Energy along the line $y = z = \pi/2$ obtained with (*solid line* and *dashed line*) or without (*dotted line*) the aid of the CTCS treatment

$x = 0.05$; here $U = (\rho, u_x, u_y, u_z, p, B_x, B_y, B_z)$. A 10 times denser spherical cloud centered at (0.25,0.5,0.5) with a radius $r = 0.15$ is in hydrostatic equilibrium with the surrounding state. The profile of the initial mass density is shown in Fig. 4 (left). The numerical solution is computed at time $t = 0.06$ using the Cartesian dual cell scheme along with its corresponding CTCS divergence treatment; the maximum absolute value of the divergence observed remains within the 10^{-12} values (Fig. 5d). An equivalent variant of

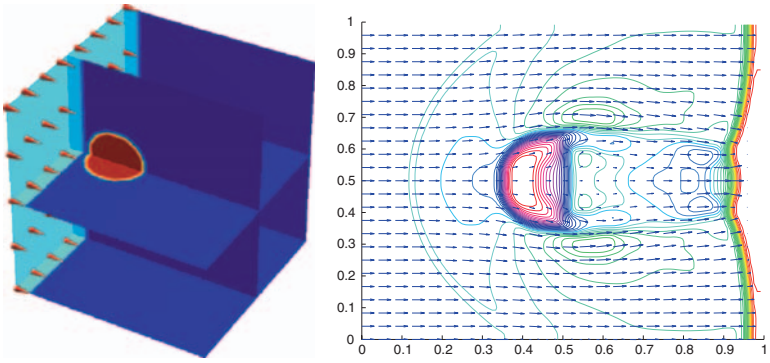

Fig. 4. (*Left*) Initial mass density profile for the 3D shock-cloud interaction problem; we also see the velocity field magnitude as a cone plot. (*Right*) Several contour lines of the mass density logarithm at time $t = 0.06$

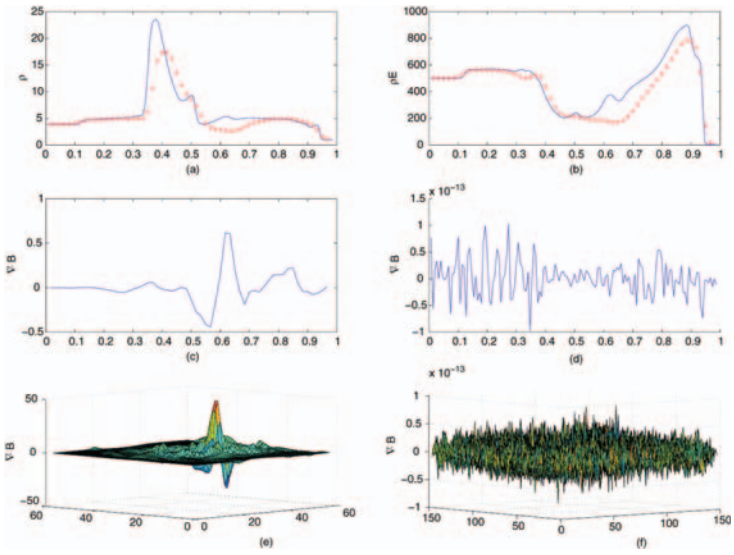

Fig. 5. Shock-cloud interaction problem: (**a**) plot of the mass density along the line $y = z = 0.5, 0 \leq x \leq 1$ obtained using the base scheme with the CTCS (150 points, *solid line*) and without any divergence treatment (60 points, *dotted line*); (**b**) same comparison for the energy

this three-dimensional problem is considered in [Z04]. Figure 4 (right) shows several contour lines of the mass density. Figure 5a shows a plot of the mass density using the Cartesian dual cell scheme with the CTCS divergence treatment and 150^3 gridpoints; the results are very similar to the reference solution presented in [27]. We have also included in this figure our results using the diamond dual cell scheme with 60^3 gridpoints and no CTCS divergence treatment. Figure 5b shows the same comparison for the energy. We observe that the base scheme does not become unstable; although $\nabla \cdot \mathbf{B}$ is not negligible (Fig. 5c, showing $\nabla \cdot \mathbf{B}$ along the line $y = z = 0.5$), the numerical solution still gives a somewhat reasonable overall approximation, with more significant deviations at gridpoints where the divergence is non-negligible (Fig. 5a,b).

5 Conclusion

We have presented three-dimensional, second-order accurate finite volume central schemes for solving systems of hyperbolic equations in the context of MHD problems. The resolution of the Riemann problems at the cell interfaces is avoided, thanks to the use of two staggered dual grids at alternate time steps. The cells of the original grid are Cartesian while those of the dual grid are either Cartesian or diamond-shaped.

To maintain a divergence-free magnetic field, we have constructed a method inspired from Evans and Hawley's Constrained Transport approach, which treats, at the end of each time step, the magnetic field obtained using our numerical base scheme. This Constrained Transport method for Central Schemes ("CTCS") applies to both Cartesian and diamond-shaped dual cell schemes and preserves the second-order accuracy of the base scheme. The divergence of the magnetic field is thus maintained under 10^{-11}.

For the ideal MHD problems we have considered here, both numerical schemes can still reach the final time and even yield reasonable results without generating instabilities, when we do not apply the CTCS procedure; but in this case, the magnetic field does not remain solenoidal and the CTCS method should in fact be applied for optimal results.

Our numerical results obtained with both base schemes are very similar, and in very good agreement with other results in the literature.

References

[AV95] Arminjon, P., Viallon, M.C.: Généralisation du schéma de Nessayahu-Tadmor pour une équation hyperbolique à deux dimensions d'espace. In: C.R. Acad. Sci. Paris, **320** (I), 85–88 (1995)

[ASV95] Arminjon, P., Stanescu, D., Viallon, M.C.: A two-dimensional finite volume extension of the Lax-Friedrichs and Nessyahu-Tadmor schemes for compressible flows. In: Hafez, M., Oshima, K. (Eds.) Proc. 6th. Int. Symp. on Comp. Fluid Dynamics, Vol. 4, 7–14 (1995)

[AT05] Arminjon, P., Touma, R.: Central Finite volume methods with constrained transport divergence treatment for ideal MHD. J. Comp. Phys., **204**, 737–759 (2005)

[DW98] Dai, W., Woodward, P.R.: A simple finite difference scheme for multi-dimensional magnetohydro-dynamical equations. J. Comp. Phys., **142**, 331–369 (1998)

[EH88] Evans, C.R., Hawley, J.F.: Simulation of magnetohydrodynamic flows: A constrained transport method. Astrophys. J., **332**, 659–677 (1988)

[JT64] Jeffrey, A., Taniuti, T.: Non-Linear Wave Propagation. Academic Press, New York (1964)

[NT90] Nessyahu, H., Tadmor, E.: Non-oscillatory central differencing for hyperbolic conservation laws. J. Comp. Phys., **87**, 408–463 (1990)

[NGL04] Nodes, C., Gritschneder, G.T., Lesch, H.: Radio emission and particle acceleration in plerionic supernova remnants. Astronomy and Astrophysics **423**, 13–19 (2004).

[PP55] Panofsky, W.K.H, Phillips, M.: Classical Electricity and Magnetism. Addisson-Wesley, Reading (Mass.), (1955)

[T05] Touma, R.: Méthodes de volumes finis pour les systèmes d'équations hyperboliques: applications en aérodynamique et en magnétohydrodynamique. PhD Thesis, Université de Montréal, Montréal (2005)

[TA06] Touma, R., Arminjon, P.: Central finite volume schemes with constrained transport divergence treatment for three-dimensional ideal MHD. J. Comp. Phys., **212**, 617–636 (2006)

[T00] Tóth, G.: The $\nabla \cdot \mathbf{B} = 0$ Constraint in Shock-Capturing Magnetohydrodynamics Codes. J. Comp. Phys., **161**, 605–652 (2000)

[Z04] Ziegler, U.: A central-constrained transport scheme for ideal magnetohydrodynamics. J. Comp. Phys., **192**, 393–416 (2004)